Full Alignment of Colloidal Objects by Programed Forcing

Brian Moths* and T. A. Witten

Department of Physics and James Franck Institute, University of Chicago, Chicago, Illinois 60637, USA

(Received 11 September 2012; published 8 January 2013)

By analysis and simulation, we demonstrate two methods for achieving complete orientational alignment of a set of identical asymmetric colloidal objects dispersed randomly in a fluid. Sedimentation or electrophoresis in a constant field can lead to partial alignment, in which the objects rotate about a common body axis, but the phases of rotation for these objects are random. We show that this phase disorder can be removed by two forms of programed forcing. First, simply alternating the forcing between two directions reduces the statistical entropy of the orientation arbitrarily. Second, the addition of a small rotating component to the applied field in analogy to magnetic resonance can lead to phase locking of the objects' orientation. We identify conditions for alignment of a broad class of generic objects and discuss practical limitations.

DOI: 10.1103/PhysRevLett.110.028301 PACS numbers: 82.70.Dd, 05.45.−a, 87.50.ch

Whenever an object responds to external forcing by periodic motion, this response gives potential utility in characterizing the object, manipulating it, or using it as a probe. A prime example is the response of a nuclear spin to a static magnetic field. The response to the field enables one to characterize the molecular environment of the spin [1] and to control the quantum state of the molecules [2]. Analogs using electrical or mechanical oscillations are well known [3–5]. These effects rely on the *coherent* response of the independent molecules constituting the sample: They all oscillate in concert [6]. Coherence enhances the observed signal, whose degradation provides further information about the constituent objects [7]. Moreover, once coherence is achieved, the objects can respond as one to further external forcing [8].

These well-known examples rely on a sharply resonant response by the individual objects. Here, we examine analogous phenomena in the complementary domain of purely dissipative responses of identical asymmetric colloidal objects dispersed in a fluid. In the simple case of sedimentation, the object is pulled by gravity acting at the center of buoyancy and by hydrodynamic drag forces over its surface. For asymmetric objects, the drag forces generally produce rotation as well as translation. This rotational sedimentation effect has aroused recent interest as a means of organizing colloidal objects [9–13]. For many objects, the sedimenting force leads to uniform rotation about a specific direction in the object that aligns with the force. Conditions for this "axial alignment" have been identified [10] and related to object shapes [9,12]. Any external field producing motion in the fluid, such as electrophoresis, produces analogous rotational effects [14], as described below.

This axial alignment under constant forcing is necessarily incomplete. Even when all the objects are rotating at the same rate about the same body axis, they all have arbitrary angular orientations about the aligning axis. Here, we show how programed time-dependent forcing can remove this disorder so that all the objects are rotating together coherently.

We explain these effects in the simple context of sedimentation of rigid asymmetric noninteracting colloidal objects. We first state the equation of motion that governs the rotation of each object. Then, we demonstrate alignment in the simplest case where the force simply alternates between two different directions. Under mild conditions, this alternating forcing leads to continually improving alignment. We quantify this alignment in terms of statistical entropy, showing that on average it decreases indefinitely. We next demonstrate alignment via a rotating transverse force. Finally, we discuss generalizations, experimental implementations, and practical limitations of this method.

For simplicity, we consider a single object immersed in an infinite viscous medium and subjected to a sedimentation force $\vec{F}(t)$ acting at a "forcing point" P in the object. We consider the regime of creeping flow [15], in which inertial forces are negligible and the force transmitted to a moving object by the medium is proportional to the object's velocity. A rotating rigid body with center-of-mass velocity $\vec{v}$ and angular velocity $\vec{\omega}$ experiences a proportional hydrodynamic force $\vec{F}$ and torque $\vec{\tau}$. This proportionality defines a dimensionless block 2×2 matrix whose 3×3 blocks $\mathbb{A}$, $\mathbb{T}$, and $\mathbb{S}$ depend only on the object:

$$\begin{bmatrix} \vec{v} \\ \vec{\omega} R \end{bmatrix} = \frac{1}{6\pi\eta R} \begin{pmatrix} \mathbb{A} & \mathbb{T}^T \\ \mathbb{T} & \mathbb{S} \end{pmatrix} \begin{bmatrix} \vec{F} \\ \vec{\tau}/R \end{bmatrix}, \tag{1}$$

where η is the viscosity of the fluid and R is the hydrodynamic radius of the object. For simplicity, below we will use units such that $6\pi\eta$ and R are unity. By choosing the forcing point P as our origin, we remove any external torque, so that any rotation arises entirely from the 3×3 "twist matrix" $\mathbb{T}$: $\vec{\omega} = \mathbb{T}\vec{F}$. The change of $\mathbb{T}$ owing to this $\vec{\omega}$ can be written as [9]

$$\dot{\mathbb{T}} = [\vec{\omega}^{\times}, \mathbb{T}]. \quad (2)$$

Here, we use the notation $\vec{\omega}^{\times}$ to denote the antisymmetric tensor corresponding to the vector $\vec{\omega}$: $[\vec{\omega}^{\times}]_{ij} - \epsilon_{ijk}\omega_k$. Alternatively, in a rotating frame that is fixed in the object, $\mathbb{T}$ becomes constant and F rotates: $\dot{F} = -\omega \times F$.

In what follows, we restrict our attention to a subclass of $\mathbb{T}$'s—denoted as "axially aligning"—that align in a unique direction, independent of initial orientation, under constant forcing. Such $\mathbb{T}$'s have sufficiently large antisymmetric parts such that they have only one real eigenvalue λ_3 and one real eigenvector $\vec{v}_3$. Then, $\mathbb{T}$ aligns with its $\vec{v}_3$ along $\vec{F}$ and rotates at angular velocity $\lambda_3\vec{F}$ [16]. An example of one such object, made by four conjoined spheres, is shown in Fig. 1(a) [17].

We first consider a minimal forcing program: a mere switch of the forcing direction by a "rocking angle" θ from its initial direction along the z axis. Figure 1(b) illustrates the result of this switch. An initially uniform distribution of phase angles ϕ becomes nonuniform; the transient relaxation has reduced the disorder.

More explicitly, we may define a basis of unit vectors $\hat{e}_1$, $\hat{e}_2$, $\hat{e}_3$ in the object whose $\hat{e}_3$ axis is the direction that aligns with the force $\vec{F}$, initially along the z axis in the lab frame [Fig. 1(a)]. At a given moment, this object's $\hat{e}_2$ vector makes an azimuthal angle ϕ with the lab's y axis. This ϕ increases steadily in time as explained above. The ϕ's of the different objects are presumed to be uniformly distributed. After $\vec{F}$ has switched into the x-z plane and the objects have realigned, their $\hat{e}_2$ vectors again differ only in their azimuthal angle with the y axis, which we denote as ψ. Evidently, an object's angle ψ at a time t after the switch depends on the angle ϕ immediately before the switch: $\psi = \psi_t(\phi)$. As the figure illustrates, the ψ angles are no longer uniformly distributed: Some ψ's have bunched closer together; others have spread apart. For convenience, we shall choose a time t so that $\psi(0) = 0$. Evidently, if the rocking angle $\theta = 0$, the motion is a continuation of the uniform rotation without any switch: $\psi(\phi) = \phi$. If θ increases from zero by a small amount, $\psi(\phi)$ remains close to ϕ and $\psi(\phi)$ remains monotonic [18]. Further, for general θ, as ϕ advances by 2π, ψ must advance by the same net amount. Thus, $2\pi = \oint d\phi(d\psi/d\phi)$ [18]. Typical $\psi(\phi)$'s are shown in Figs. 1(c)–1(e).

We may quantify the bunching effect of ψ using the probability distribution function $p(\phi)$ measured after the objects have aligned. The net effect on the distribution can be quantified using the statistical entropy [19] $H \equiv -\int p \ln p$. This H is maximal for uniform probabilities and is small when the probability is concentrated into small regions. After one switching process, each angle ϕ evolves into some $\tilde{\phi}$. The passage from ϕ to $\tilde{\phi}$ involves two steps: We first wait a random fraction of the rotational period, so that ϕ undergoes a shift by a random angle α. We then switch the force F and allow the objects to realign. The resulting angle $\tilde{\phi} = \psi(\phi + \alpha)$. The corresponding probability distribution $\tilde{p}(\tilde{\phi})$ is found using $\tilde{p}(\tilde{\phi})d\tilde{\phi} = p(\phi)d\phi$, so that $\tilde{p}(\tilde{\phi}) = p(\phi)/\psi'(\phi + \alpha)$.

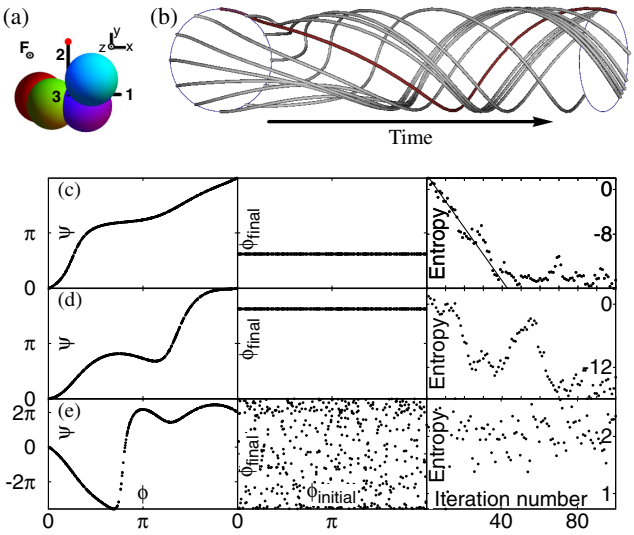

FIG. 1 (color online). (a) The conjoined-sphere object referenced in the main text axially aligned to a downward force $\vec{F}$, viewed from slightly below the horizontal. A lab basis x-y-z and a body basis $\hat{e}_1$, $\hat{e}_2$, $\hat{e}_3$, centered at the forcing point, are shown. The azimuthal angle ϕ is 0. The object's $\mathbb{T}$ matrix in $\hat{e}_1$, $\hat{e}_2$, $\hat{e}_3$ coordinates was computed using the HYDROSUB software package [25]. A colored dot marks the $\hat{e}_2$ axis. (b) Motion after a switch in force direction. The darker line illustrates the trajectory of the colored dot after the forcing direction has switched to the x direction. Eleven other trajectories for objects initially rotated by different ϕ's are also shown. After realignment, the points have become nonuniformly distributed on the new circle. (c)–(e) Sample results of repeated rocking by 90 degrees as described in the text. The left-hand graphs show the mapping function $\psi(\phi)$. The center graphs show the angles ϕ for 100 randomly oriented copies of the object after 100 switches. The right-hand graphs show the progression of the entropy H with repeated rocking. The final low values are consistent with the noise floor of the numerics. (c) shows the results of a monotonic ψ function. The line indicates the predicted slope from (4). (d) shows the results for the object shown in (a). (e) shows the results for a strongly nonmonotonic $\psi(\phi)$ whose entropy does not decrease.

We now show that, if θ is chosen so small that ψ' is everywhere positive, repeatedly switching $\vec{F}$ causes the entropy to decrease without bound. For a single switch, the change in entropy ΔH depends on the shift angle α [18]:

$$\Delta H_\alpha = \oint p(\phi) \ln[\psi'(\phi + \alpha)] d\phi. \quad (3)$$

We now consider the net change of H after a sequence of many switches of F. Then, the α-averaged change of H, $\langle \Delta H \rangle$, can be written as

$$\langle \Delta H \rangle = \oint p(\phi + \alpha) \ln[\psi'(\phi)] d\phi. \quad (4)$$

The $\langle p(\phi + \alpha) \rangle$ is an unimportant positive constant. The remaining integral is a constant that is necessarily negative [19], owing to the convexity of the logarithm. Thus, after many switches, the entropy must decrease indefinitely on average and the probability p becomes confined to arbitrarily small regions of ϕ. As Figs. 1(c) and 1(d) illustrate, the initial set of ϕ's often evolves into a single final ϕ [20]. Further, this reduction of H often occurs even when ψ' is not positive definite [Fig. 1(d)]. Given a mixture of two or more alignable species, this method aligns each species. However, one readily finds examples $\psi(\phi)$ where the entropy does not decrease [Fig. 1(e)]. In any case, the direction of alignment is not controlled in this method.

A second method of forcing can achieve alignment in a controlled direction. We add a rotating transverse force to the original static force so that the force vector is tilted at an angle θ from the z axis. Thus, $\vec{F}$ rotates at a constant angular velocity $\vec{\Omega} = |\Omega|\hat{z}$:

$$\vec{F}(t) = |F|(\hat{z}\cos\theta + [\hat{x}\cos\Omega t + \hat{y}\sin\Omega t]\sin\theta). \quad (5)$$

In a *corotating* frame rotating at angular velocity $\vec{\Omega}$, the force $\vec{F}$ becomes constant. With a proper choice of Ω and θ, the objects, too, may evolve into a state of corotation with the force, with a common orientation. Corotation requires that $\mathbb{T}$ remain in an orientation such that $\vec{\Omega} = \mathbb{T}\vec{F}$. As noted above, a fixed force with $\theta = 0$ leads to corotation with $\vec{\Omega} = \lambda_3 \vec{F}$. In the $\hat{e}_1$, $\hat{e}_2$, $\hat{e}_3$ body reference frame, denoted with subscript b, corotation means $\vec{\Omega}_b = \mathbb{T}_b \vec{F}_b$ for some constant $\vec{F}_b$ and corresponding $\vec{\Omega}_b$. The forcing parameters required are evidently (a) $|F|^2 = |F_b|^2$, (b) $|\Omega|^2 = |\Omega_b|^2$, and (c) $\cos\theta = \hat{F}_b \cdot \hat{\Omega}_b$.

With this same choice of parameters, other corotating $\vec{F}$'s are also possible. We denote these as $\vec{F}'_b$. Because of condition (a), such $\vec{F}'_b$'s have the same magnitude as $\vec{F}$, so that the only difference in the $\vec{F}_b$'s is in their direction $\hat{F}'_b$. In terms of the matrix $\mathbb{T}_b$, condition (b) can be written as $\hat{F}'_b {\mathbb{T}_b}^T \mathbb{T}_b \hat{F}'_b = \hat{F}_b {\mathbb{T}_b}^T \mathbb{T}_b \hat{F}_b (= |\Omega|^2/|F|^2)$. (If $\hat{F}'_b$ satisfies this condition, so does $-\hat{F}'_b$.) This condition restricts $\hat{F}'_b$ to two (closed) curves on the unit sphere like the dashed line in Figs. 2(a)–2(c). Likewise, condition (c) reads $\hat{F}'_b \mathbb{T}_b \hat{F}'_b / |\mathbb{T}_b \hat{F}'_b| = \hat{F}_b \mathbb{T}_b \hat{F}_b / |\mathbb{T}_b \hat{F}_b| (= \cos\theta)$. This condition restricts $\hat{F}'_b$ to a second pair of curves on the unit sphere. Any intersection of these curves represents an $\hat{F}'_b$ that corotates with the given forcing.

These compatible F_b's can readily be found when the tilt angle θ is small. Figures 2(a)–2(c) show the behavior of the corotating $\hat{F}'_b$'s as one increases θ from 0 with $|\Omega| = \lambda_3 F$. The condition (b) curves, enforcing the magnitude of Ω, are thus independent of θ and do not change. These curves pass through $\hat{e}_3$ and $-\hat{e}_3$, i.e., the $\hat{F}_b$ for $\theta = 0$. Condition (c), enforcing $\cos\theta$, requires $\hat{F}_b \parallel \hat{e}_3$ when $\theta = 0$. As θ increases, the condition (c) curves expand to small rings encircling $\pm\hat{e}_3$. Each ring must intersect its condition (b) curve twice. The four corotating $\hat{F}'_b$'s are then two adjacent pairs near $\pm\hat{e}_3$. In what follows, we consider only the two intersections adjacent to the stable $+\hat{e}_3$ direction.

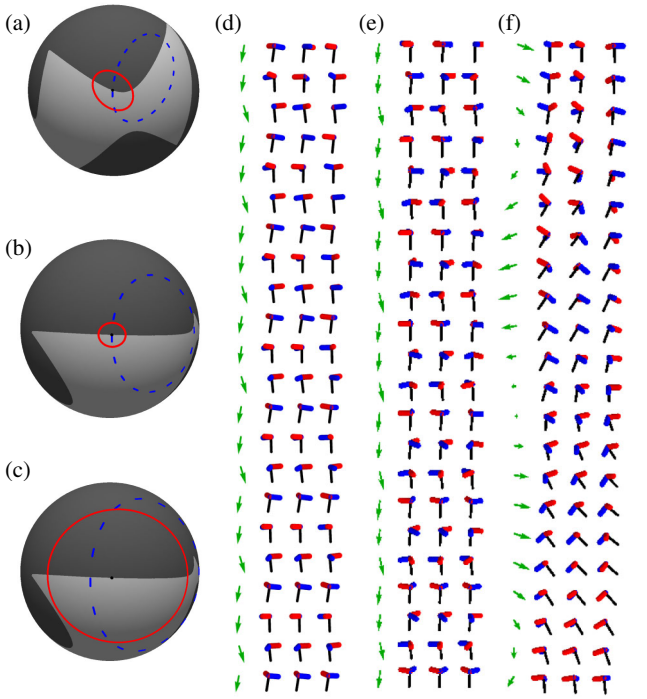

FIG. 2 (color online). (a) The sphere of possible directions of the body frame force $\vec{F}_b$ for the object of Fig. 1(a). The solid curve gives the $\hat{F}'_b$'s satisfying constraint c in the text, enforcing an angle $\theta = 0.3$. The dashed curve gives the $\hat{F}$'s satisfying constraint b in the text, enforcing $|\Omega| = \lambda_3|F|$. The intersections of the two curves mark corotating states. The light shading marks regions of stable fixed points $\hat{F}_b$ for this object. (b) Same as (a) for the $\mathbb{T}$ used for Fig. 1(e) with $\theta = 0.2$. (c) Same as (b), with $\hat{F}_b$ chosen to lie far from the aligning direction $\hat{e}_3$ to illustrate alignment with a large tilt angle. Here, $|\Omega \neq \lambda_3|F|$; instead, $\vec{\Omega}_b = \mathbb{T}_b \vec{F}_b$. (d) Time sequence of orientations using the object and alignment protocol described in (a). Three arbitrarily oriented copies of the object, represented by their $\hat{e}_1$, $\hat{e}_2$, $\hat{e}_3$ bases, are shown. Colored arrows indicate the direction of forcing. The three objects evolved to a common final orientation. (e) Similar time sequence for the $\mathbb{T}$ matrix used for Fig. 1(e). (f) Similar time sequence for the $\mathbb{T}$ matrix and forcing condition shown in (c).

To achieve full alignment, an arbitrary initial state must evolve into one of these two corotating states. We argue that this alignment occurs generally for sufficiently small θ. We consider the motion of $\mathbb{T}$ in the corotating frame, in which $\vec{F}$ and $\vec{\Omega}$ are fixed. We first align $\mathbb{T}$ axially using a constant $\vec{F}$. We can express the orientation of $\mathbb{T}$ using a rotation vector $\vec{\eta}$. We distinguish angular rotations η_3 along the $\vec{\Omega}$ axis from rotations $\eta_\perp$ perpendicular to it.

In this initial state, $\eta_\perp = 0$, while the orientation η_3 about the aligning axis is arbitrary: Axial alignment has restricted $\vec{\eta}$ to a closed one-dimensional curve of possible values. A small rotation η_3 has no further effect on the motion, but a small rotation $\eta_\perp$ leads to a stable return to $\eta_\perp = 0$.

Now, we increase θ to a small nonzero value. Then, $\vec{\eta}$ is no longer constant. The time derivative $\dot{\vec{\eta}}_\theta(\vec{\eta})$ differs from $\dot{\vec{\eta}}_0(\vec{\eta})$ by a small smooth perturbation. We now suppose that $\eta_\perp$ converges to some η_3-dependent value near 0. The remaining motion is along a one-dimensional closed curve, slightly distorted from the neutral curve found at $\theta = 0$. We may express this residual one-dimensional motion using the coordinate η_3, whose time derivative is some function $\dot{\eta}_{3\theta}(\eta_3)$. The two fixed points identified above are necessarily fixed points η_3^*, with $\dot{\eta}_3(\eta_3^*) = 0$. Since $\dot{\eta}_{3\theta}$ is a smooth function on the curve, its derivatives at these two fixed points are necessarily opposite in sign and, hence, opposite in stability. Thus, in this picture, all η_3 must converge to the stable η_3^*. Numerical studies like those of Fig. 1 confirmed this finding for numerous asymmetric $\mathbb{T}$'s.

A local stability analysis confirms the opposite stabilities of the two fixed points $\hat{F}_b$ near $\hat{e}_3$. Starting from a given forcing with a corresponding $\hat{F}_b$, we rotate $\mathbb{T}$ by a slight angular displacement $\vec{\eta}$ from its fixed-point state $\mathbb{T}^*$ in the corotating frame so that $\mathbb{T} = \mathbb{T}^* + [\vec{\eta}^\times, \mathbb{T}^*]$. The undisplaced state $\vec{\eta} = 0$ is corotating, so that $\dot{\vec{\eta}} = 0$. Near $\vec{\eta} = 0$, $\dot{\vec{\eta}}$ varies linearly with η: $\dot{\vec{\eta}} = \mathbb{K}\vec{\eta}$ for some "stability matrix" $\mathbb{K} = [\mathbb{T}^*\vec{F}^\times - (\mathbb{T}^*\vec{F})^\times]$ [18]. From this $\mathbb{K}$, one may determine by standard methods [22] whether the motion returns stably to the corotating state at $\mathbb{T}^*$ after the small displacement $\vec{\eta}$; indeed, one finds that the two fixed points of the previous paragraph have opposite stabilities. Figures 2(a)–2(c) use this $\mathbb{K}$ to determine which $\hat{F}_b$ represent stable corotating states. The figure shows large stable and unstable regions of $\hat{F}_b$. We note that the aligning axis $\hat{e}_3$, being neutrally stable, lies at the boundary between the stable and unstable regions.

These alignment methods are applicable for any situation where an object responds to a vector field by rotating. For example, any asymmetric object with an electrophoretic mobility has such a rotational response [14]. Programed forcing via tensor interactions such as field gradients or shear flow adds further possibilities for alignment. Any proportional response to vector forcing is necessarily governed by a $\mathbb{T}$ matrix like that above. This is true for deformable objects whenever the driving force is weak enough to avoid deformation. It is true for fluctuating shapes whenever the driving is weak enough to average over the fluctuations of $\mathbb{T}$.

Complete alignment brings benefits that are not possible in axial alignment. Once a set of objects has been completely aligned, they must respond identically to subsequent forcing. Then, e.g., by gradually increasing the Ω of Eq. (5), one may achieve phase locking without knowing about the $\mathbb{T}$ of the objects in advance [18]. Further extensions of programed phoresis hold promise for orienting nonaxially aligning objects not considered here.

In practice, alignment is degraded by rotational diffusion, characterized by a relaxation time τ_D, which scales as the cube of the object's size R [15]. For alignment, the rotational speed ω must be much larger than $1/\tau_D$. Thus, under sedimentation, alignment is strongly degraded as R is decreased: $\omega\tau_D \sim R^4$. The asymmetric object of Fig. 1(a) has $\omega\tau_D \simeq 260$ [17]. Under electrophoresis, an object with a nominal mobility of 10^{-8} m/(V s) and field of 10^4 V/m would need to be over 10 microns in size to give comparable $\omega\tau_D$. Thus, these methods require objects of near-micron scale or larger. Since alignment effects require object asymmetry, nearly symmetric objects are harder to align.

Unless the objects are very dilute [23], their mutual hydrodynamic interactions would be significant: An object B is advected by the perturbed Oseen flow around a nearby object A [24]. Only the gradient of this flow *rotates* object B. The rotational perturbations on an object are thus shorter range and hence weaker than are translational hydrodynamic interactions. Ordinary electrophoresis produces no Oseen flow in the host fluid [14]; thus, electrophoresis is less subject to interaction effects.

The authors thank Michael Solomon for his suggestion that this work is applicable to electrophoresis, Nathan Krapf for valuable guidance, and Michael Cates and our referees for useful comments on the manuscript. This work was supported in part by the National Science Foundation's MRSEC Program under Grant No. DMR-0820054.

*bmoths@uchicago.edu

[1] J. M. Seco, E. Quiñoá, and R. Riguera, Chem. Rev. **104**, 17 (2004).
[2] W. Happer, E. Miron, S. Schaefer, D. Schreiber, W. A. van Wijngaarden, and X. Zeng, Phys. Rev. A **29**, 3092 (1984).
[3] D. Vion, A. Aassime, A. Cottet, P. Joyez, H. Pothier, C. Urbina, D. Esteve, and M. H. Devoret, Science **296**, 886 (2002).
[4] G. D. Fuchs, A. L. Falk, V. V. Dobrovitski, and D. D. Awschalom, Phys. Rev. Lett. **108**, 157602 (2012).
[5] B. Abbott *et al.*, Nucl. Instrum. Methods Phys. Res., Sect. A **517**, 154 (2004).
[6] N. Bloembergen, E. Purcell, and R. Pound, Phys. Rev. **73**, 679 (1948).
[7] R. Riek, G. Wider, K. Pervushin, and K. Wüthrich, Proc. Natl. Acad. Sci. U.S.A. **96**, 4918 (1999).
[8] C. J. Bardeen, V. V. Yakovlev, K. R. Wilson, S. D. Carpenter, P. M. Weber, and W. S. Warren, Chem. Phys. Lett. **280**, 151 (1997).
[9] N. W. Krapf, T. A. Witten, and N. C. Keim, Phys. Rev. E **79**, 056307 (2009).
[10] O. Gonzalez, A. Graf, and J. Maddocks, J. Fluid Mech. **519**, 133 (2004).
[11] M. Makino and M. Doi, J. Phys. Soc. Jpn. **72**, 2699 (2003).
[12] M. Doi and M. Makino, Phys. Fluids **17**, 043601 (2005).

[13] A. V. Andreev, D. T. Son, and B. Spivak, Phys. Rev. Lett. **104**, 198301 (2010).
[14] D. Long and A. Ajdari, Phys. Rev. Lett. **81**, 1529 (1998).
[15] J. Happel and H. Brenner, *Low Reynolds Number Hydrodynamics: With Special Applications to Particulate Media* (Prentice-Hall, Englewood Cliffs, NJ, 1965).
[16] In practice, many nonsymmetric objects are axially aligning [9].
[17] The buoyant masses from closest to farthest are in the ratio 1.34, 0.80, 0.72, 1.14. For this object, up to a numerical factor,

$$\mathbb{T} \simeq \begin{pmatrix} -0.46 & -0.71 & 0 \\ 0.25 & -0.41 & 0 \\ 0.23 & 0 & 1 \end{pmatrix}.$$

In a 10^4 g centrifuge, this object with spheres of 1 micron diameter and specific gravity of 1.1 in water would rotate at 25 rad/sec.
[18] B. E. Moths and T. A. Witten (to be published).
[19] C. E. Shannon, *The Mathematical Theory of Communication* (University of Illinois Press, Urbana, 1948).
[20] Kaijser [21] argues that the probabilities *must* collapse to a single point.
[21] T. Kaijser, Physica (Amsterdam) **68D**, 201 (1993).
[22] S. Strogatz, *Nonlinear Dynamics and Chaos: With Applications to Physics, Biology, Chemistry, and Engineering*, Studies in Nonlinearity (Westview, Cambridge, MA, 2001).
[23] With sufficient dilution, hydrodynamic interactions take arbitrarily long to manifest compared to alignment effects, the latter being dilution independent.
[24] J. Z. Xue, E. Herbolzheimer, M. A. Rutgers, W. B. Russel, and P. M. Chaikin, Phys. Rev. Lett. **69**, 1715 (1992).
[25] J. García de la Torre and B. Carrasco, Biopolymers **63**, 163 (2002).